ARTICLES

Optical and transport studies of $Ni(dmit)_2$-based organic conductors

H. L. Liu and D. B. Tanner
Department of Physics, University of Florida, Gainesville, Florida 32611

A. E. Pullen, K. A. Abboud, and J. R. Reynolds
Department of Chemistry, Center for Macromolecular Science and Engineering, University of Florida, Gainesville, Florida 32611

(Received 9 November 1995)

Single-crystal $Ni(dmit)_2$ salts, $(Ph_4P)[Ni(dmit)_2]_3$, $(Bu_4N)_2[Ni(dmit)_2]_7 \cdot 2CH_3CN$, and $(Me_3S)[Ni(dmit)_2]_2$, have been synthesized. All show semiconducting behavior in their temperature-dependent dc conductivities. Room-temperature polarized reflectance measurements have been made over the range between 100 and 32 000 cm^{-1} (12 meV–4 eV). For light polarized along the $Ni(dmit)_2$ stacking axis, all spectra show an energy gap, with superimposed vibrational fine structure at low frequencies and charge-transfer bands at high frequencies. Band gaps determined from the optical conductivities are consistent with thermal activation energies from dc transport measurements. The stacking-axis conductivity shows the effect of electron-molecular vibration interaction; analysis for $(Me_3S)[Ni(dmit)_2]_2$ yields a dimensionless electron-phonon coupling constant $\lambda \sim 0.27$. For light polarized perpendicular to the stacking axis, only weak vibrational features are observed.

I. INTRODUCTION

In 1973, an organic charge-transfer complex composed of the donor molecule TTF (tetrathiafulvalene) and the acceptor molecule TCNQ (7,7,8,8-tetracyano-*p*-quinodimethane) was synthesized and found to display metalliclike electronic properties.[1] Since this remarkable discovery, much research has gone into the design, synthesis, and characterization of new charge-transfer salts. Systems are known that show not only semiconducting and metallic behavior, but also superconductivity. Most organic superconductors are based either on TMTSF (tetramethyltetrathiafulvalene)[2] or BEDT-TTF [bis(ethylenedithio)tetrathiafulvalene].[3] In addition to these molecular conductors based on multisulfur π-donor molecules, salts based on multisulfur π-acceptor molecules have begun to attract increasing interest.

A unique family of complexes derived from $[Ni(dmit)_2]^{n-}$ (where dmit=1,3-dithiole-2-thione-4,5-dithiolato) with $0 \leqslant n \leqslant 2$ has recently received attention.[4] The electronic properties of the $Ni(dmit)_2$ acceptor complexes are attributed to the nonbonding interactions of the acceptor entities. By using planar ligands and square-planar coordinating transition metals, close packing arrangements are formed in the crystal. With ten sulfur atoms along the periphery of the planar ligands, S···S overlap can be large. These structural effects promote strong intermolecular interactions and suppress the Peierls distortion, leading to high electrical conductivity. Three superconducting $Ni(dmit)_2$ complexes have been reported. The first, $TTF[Ni(dmit)_2]$, shows high electrical conductivity at ambient pressure 300 Ω^{-1} cm^{-1} at 300 K to $\sim 10^5$ Ω^{-1} cm^{-1} at 4.2 K. Furthermore, under 7 kbar pressure, this compound superconducts with a $T_c = 1.62$ K.[5] The second salt, $(Me_4N)[Ni(dmit)_2]_2$, is metallic ~ 50 Ω^{-1} cm^{-1} at room temperature and becomes superconducting at 5 K under 7 kbar.[6] Finally, the ambient pressure superconductor complex α-EDT-TTF$[Ni(dmit)_2]$ displays metalliclike electrical conductivity down to 1.3 K where it becomes superconducting.[7]

In order to provide further information on the nature of $Ni(dmit)_2$ complexes, we have used electrocrystallization techniques to synthesize three $Ni(dmit)_2$-based donor-acceptor compounds with closed-shell cations, $(Ph_4P)[Ni(dmit)_2]_3$,[8,9] $(Bu_4N)_2[Ni(dmit)_2]_7 \cdot 2CH_3CN$,[10] and $(Me_3S)[Ni(dmit)_2]_2$,[8,11] and measured their transport and optical properties. To our knowledge, despite the large number of interesting $Ni(dmit)_2$ salts, relatively few optical studies have been made.[9,12–17] In this paper we describe the comprehensive transport and optical properties of these three organic materials. Spectroscopic methods are well suited to the study of such highly anisotropic crystals, providing information on both the electronic charge transfer and localized excitations at high energies as well as the vibrational features at low energies.[18] Eight infrared-active vibrational modes in the $Ni(dmit)_2$ stacking direction are of particular interest. Infrared activity of these modes can be attributed to the coupling of the totally symmetric (A_g) $Ni(dmit)_2$ vibrational modes with low-lying electronic charge-transfer excitations;[19] it is very sensitive to changes in the electronic structure of the crystal. Emphasis has been placed on the correlation of the spectral properties with available structural and transport data. In addition, we compare our data on $(Ph_4P)[Ni(dmit)_2]_3$ to earlier results by Nakamura *et al.*[9]

II. EXPERIMENT

A. Material synthesis

The $dmit^{2-}$ ligand was prepared following the procedures described by Steimecke *et al.*[20] The complex

TABLE I. Structural parameters for $[Ni(dmit)_2]$ salts.

	$(Ph_4P)[Ni(dmit)_2]_3$	$(Bu_4N)_2[Ni(dmit)_2]_7\cdot 2CH_3CN$[a]	$(Me_3S)[Ni(dmit)_2]_2$
Space group	C_2	P-1	P-1
Crystal system	Monoclinic	Triclinic	Triclinic
a (Å)	18.114(2)	13.604(2)	7.923(1)
b (Å)	7.193(1)	22.965(3)	11.647(1)
c (Å)	22.960(4)	24.270(4)	17.812(2)
$\alpha°$	90.00(0)	108.16(1)	77.46(1)
$\beta°$	92.60(1)	103.09(1)	85.93(1)
$\gamma°$	90.00(0)	89.67(1)	81.36(1)
V (Å^3)	2988.5(7)	7000	1585.0(3)
Z	2	2	2

[a]From Ref. 10.

$(Ph_4P)[Ni(dmit)_2]_3$ was synthesized *via* constant current electrocrystallization in CH_3CN with 0.075M Ph_4PBr electrolyte. A current density of 1.5 μA/cm^2 was used over a period of 15 d.[8] The complex $(Bu_4N)_2[Ni(dmit)_2]_7\cdot 2CH_3CN$ was electrocrystallized in CH_3CN with 0.1M Bu_4NClO_4 electrolyte using a method similar to that of Valade *et al.*[10] A current density of 1.3 μA/cm^2 was used over a period of 24 d. Platelet and needlelike crystals were obtained upon harvesting. Platelets were chosen for study. The stoichiometry was confirmed by elemental analysis.[21] The complex $(Me_3S)[Ni(dmit)_2]_2$ was electrocrystallized in 1:1 acetone-CH_3CN with 0.1M Me_3SBF_4 electrolyte using a method similar to that of Kato *et al.*[11] We used a current density of 0.5 μA/cm^2 over a period of 26 d.[8]

B. Materials characterization

1. Structure

All structures were solved by direct methods in SHELXTL plus[22] from which the locations of the non-H atoms were obtained. The structures were refined in SHELXTL plus using full-matrix least squares. The non-H atoms were treated anisotropically. Crystal data are collected in Table I.

The crystal packing array of the $Ni(dmit)_2$ units in $(Ph_4P)[Ni(dmit)_2]_3$ is unique among the $Ni(dmit)_2$ complexes. It is shown in Figs. 1 and 2. The structure can be described as segregated, slightly staggered stacks of the planar $Ni(dmit)_2$ acceptor molecules along [010], separated ''side by side'' by planes of orthogonal spacers of the $Ni(dmit)_2$ acceptor. The acceptor stacks and spacers are separated ''end to end'' by closed-shell Ph_4P^+ donors also in the [010] direction.

There is an extensive amount of nonbonding orbital interactions exhibited throughout the structure. Looking within the segregated stacks of $Ni(dmit)_2$ acceptor units, there is no S···S orbital overlap observed. However, there is Ni d_z^2···S orbital overlap. As can be seen from Fig. 2 the interplanar acceptor spacings are equidistant at ~3.76 Å. The orthogonal spacer acceptor units have a separation of 4.058 Å, which results in intermolecular interspacer S···S distances well beyond the sum of the van der Waals radii of 3.70 Å. Despite the fact that there are no interspacer or interstack S···S interactions, there is a significant amount of spacer-stack interactions. Each $Ni(dmit)_2$ spacer unit interacts with the six $Ni(dmit)_2$ units within adjacent stacks. The Ni d_z^2 orbital of the spacers is directed toward the thiolate sulfurs of $Ni(dmit)_2$ units in the two neighboring molecules. The spacing between stack and spacer is 3.426 Å. A number of spacer-stack interactions are also observed involving the peripheral thiolate and thiole groups of the $Ni(dmit)_2$ spacers.

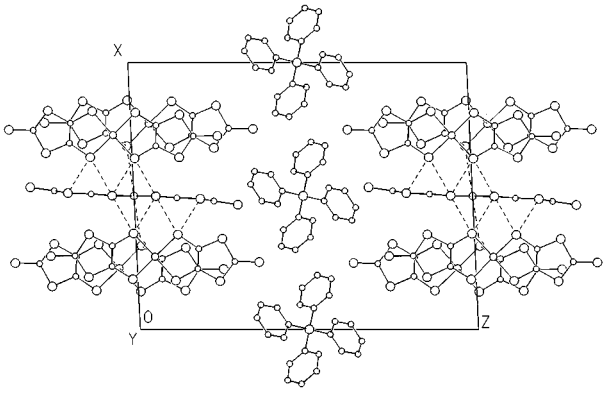

FIG. 1. View down the b axis of (Ph_4P) $[Ni(dmit)_2]_3$. The dotted lines represent S···S and Ni···S distances that are less than the sum of the van der Waals radii.

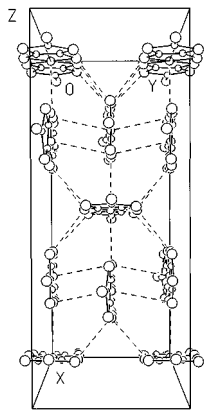

FIG. 2. View down the c axis of (Ph_4P) $[Ni(dmit)_2]_3$ showing the array of stacks and orthogonal spacer $Ni(dmit)_2$ units. (Ph_4P^+ cations have been removed for clarity.) Dotted lines represent nonbonding interactions.

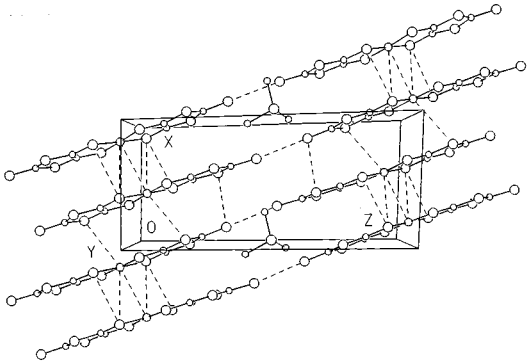

FIG. 3. View down the *b* axis of $(Me_3S)[Ni(dmit)_2]_2$. The dotted lines represent nonbonding interactions.

Each of these groups interact with two $Ni(dmit)_2$ units within the adjacent stacks. The separations range from 3.609 to 3.628 Å; all are shorter than the van der Waals separation of 3.70 Å. Along the [001] direction, there are no nonbonding interactions observed between the terminal thione groups of the acceptor and Ph_4P^+ donor units. Therefore, $(Ph_4P)[Ni(dmit)_2]_3$ has a quasi-two-dimensional network of S···S and Ni d_z^2···S intermolecular interactions. Note that our structure compares rather well with that already reported by Nakamura *et al.*[9] except that we have chosen the *c* axis as half of theirs due to difficulties with data collection, and subsequent data resolution, on a unit cell where one axis is more than 45 Å in length. The structure was solved and refined in the *C*2 space group and showed no signs of disorder. The final refinement yielded *R* and *wR* values of 4.55 and 4.61, respectively for I and 3.29 and 3.96 for II.

Several groups have reported different stoichiometries for $(Bu_4N)_2[Ni(dmit)_2]_7\cdot CH_3CN$.[4] According to Valade *et al.*,[10] this complex has the stoichiometry $(Bu_4N)_2[Ni(dmit)_2]_7\cdot 2CH_3CN$ based on x-ray and elemental analysis. The structure can be described as consisting of thick layers of $Ni(dmit)_2$ entities oriented parallel to (001) and separated by sheets of Bu_4N^+ cations and CH_3CN molecules. Within a layer the $Ni(dmit)_2$ species are arranged in stacks along the [110] direction. A stack consists of quasiparallel quasiplanar $Ni(dmit)_2$ units arranged in alternating centrosymmetric triads and tetrads. The axes of the triads and tetrads are parallel but make an angle of about 21° with the overall stacking direction [110]. Given the π interactions along the stacks on the one hand and the interstack S···S interactions on the other, it is clear that the structure arrangement of $(Bu_4N)_2[Ni(dmit)_2]_7\cdot 2CH_3CN$ cannot be viewed as a classical one-dimensional system but is much more nearly two dimensional.

The structure of $(Me_3S)[Ni(dmit)_2]_2$ is characterized by segregated stacks of acceptor $Ni(dmit)_2$ units and Me_3S^+ units along [100] as shown in Fig. 3. Each $Ni(dmit)_2$ unit exhibits nonbonding interactions with seven other $Ni(dmit)_2$ units within the lattice. This results in not only intrastack interactions of $Ni(dmit)_2$ units, but also ''side-by-side'' and ''end-to-end'' interstack interactions. An important feature of the lattice is the presence of two independent alternating interplanar distances, forming a quasidimer system within the stacks. Examining the intradimer $Ni(dmit)_2$ unit spacings within a stack, the shortest S···S value is 3.491 Å. Interdimer nonbonding interactions are also present as the S···S separation distance values range from the shortest, 3.58 Å, to the longest at 3.644 Å.

As mentioned already, ''side-by-side'' and ''end-to-end'' nonbonding interactions are prevalent in the lattice. Adjacent stacks of $Ni(dmit)_2$ units have separations in the range of 3.514 to 3.657 Å. The terminal thione groups also exhibit nonbonding interactions on the order of 3.571 Å. Therefore, $(Me_3S)[Ni(dmit)_2]_2$ appears to have a quasi-three-dimensional network of S···S and Ni···S intermolecular interactions.

2. Transport measurements

Temperature-dependent (300–10 K) resistances were measured by a four-probe method, using an ac technique. Five different needle-shaped crystals of $(Ph_4P)[Ni(dmit)_2]_3$ (typically $3.5\times0.2\times0.04$ mm^3) and two each of $(Bu_4N)_2[Ni(dmit)_2]_7\cdot 2CH_3CN$ ($3\times0.1\times0.05$ mm^3) and $(Me_3S)[Ni(dmit)_2]_2$ ($3\times0.5\times0.05$ mm^3) were measured. Narrow gauge (0.02-mm diameter) gold wires were affixed to the crystal under a microscope using fast drying gold paint. The sample was thermally anchored to the cold head of a closed-cycle refrigerator (CTI Cryogenics). A typical run was done by first cooling the sample to the lowest temperature, and then taking the data while warming. Temperature reproducibility has been determined to be ±0.2 K or better over the temperature range measured.

3. Optical spectroscopy

Near-normal polarized reflectance measurements were made on single-crystal samples. Far-infrared and midinfrared measurements were carried out on an Bruker 113v Fourier-transform infrared spectrometer using a 4.2-K bolometer detector (30–600 cm^{-1}) and a B-doped Si photoconductor (450–4000 cm^{-1}). Wire grid polarizers on polyethylene and AgBr were used in the far and midinfrared, respectively. A Perkin-Elmer 16U grating spectrometer in conjunction with thermocouple, PbS, and Si detectors was used to measure the spectra in the infrared to the ultraviolet (1000–32 000 cm^{-1}), using wire grid and dichroic polarizers.

Experiments were performed with light polarized parallel and perpendicular to the $Ni(dmit)_2$ stacking axis. The reflectance was calibrated with a reference aluminum mirror. In order to correct for size differences between sample and reference and to compensate for scattering losses, all samples were coated with a thin aluminum layer after the optical measurements were finished. The final corrected reflectance was obtained by rationing the initial reflectance (no coating) to the reflectance of the coated sample, then multiplying the ratio by the aluminum reflectance. After the reflectance spectra were measured, the optical properties were determined by Kramers-Kronig analysis.[23] Because an extremely large frequency region was covered, Kramers-Kronig analysis should provide reasonably accurate values for the optical constants. To perform these transformations one needs to extrapolate the reflectance at both low and high frequencies. At very low frequencies the reflectance was assumed constant. Between the highest-frequency data point and 10^6 cm^{-1}, the reflectance was assumed to follow a power law of ω^{-1}, beyond this frequency range a free-electron-like behavior of ω^{-4} was used.

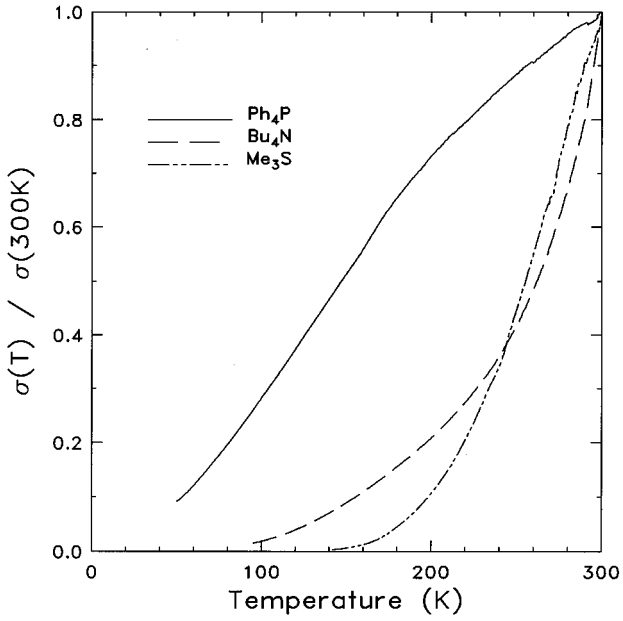

FIG. 4. The dc conductivity normalized by its room-temperature value for $(Ph_4P)[Ni(dmit)_2]_3$, $(Bu_4N)_2[Ni(dmit)_2]_7\cdot 2CH_3CN$, and $(Me_3S)[Ni(dmit)_2]_2$ vs temperature.

III. RESULTS

A. Transport properties

Temperature-dependent four-probe electrical conductivity measurements are shown in Fig. 4. Semiconducting behavior is found for all of the compounds investigated. The conductivity decreases from its 300-K value when temperature is decreased. The typical temperature dependence of the conductivity may be expressed as

$$\sigma(T)=\sigma_0 e^{-E_g/2k_BT}, \tag{1}$$

where E_g is the semiconductor gap. The values of room-temperature conductivity and the thermal activation energy $E_a=E_g/2$ are listed in Table II.[4,9,10,24–26] The results for our materials are compared to those observed previously for $[Ni(dmit)_2]$ salts with different closed-shell organic cations. For $(Ph_4P)[Ni(dmit)_2]_3$ our room-temperature conductivity agrees with that published by Nakamura *et al.*[9] However, the thermal activation energy measured in this work is smaller than found by Nakamura *et al.*[9] In contrast, our conductivity parameters for $(Bu_4N)_2[Ni(dmit)_2]_7\cdot 2CH_3CN$ coincide with the prior Valade *et al.*[10] data. Interestingly, both $(Ph_4P)[Ni(dmit)_2]_3$ and $(Bu_4N)_2[Ni(dmit)_2]_7\cdot 2CH_3CN$ have high conductivities and low activation energies. This suggests the presence of fractional oxidation states. An additional result is that there is a change in the apparent activation energy around 100 K in $(Ph_4P)[Ni(dmit)_2]_3$. The plot of $\ln\sigma$ versus $1/T$ does not obey a single linear relationship; instead two different slopes were obtained above and below a crossover point of 100 K. E_a is smaller at low temperature, probably due to impurity effects. Another formula for the conductivity comes from the model proposed by Epstein and Conwell,[27,28]

$$\sigma(T)=ne\mu(T)=\sigma_0 T^{-\alpha}e^{-E_g/2k_BT}, \tag{2}$$

where $\mu(T)\simeq\mu_0 T^{-\alpha}$ and $n\propto e^{-E_g/2k_BT}$. The conductivity is a product of a strongly temperature-dependent mobility and an activated carrier concentration. A fit of this model to our experimental results did not give a single activation energy for $(Ph_4P)[Ni(dmit)_2]_3$.

B. Optical results

1. Polarized reflectance

Figure 5 shows the polarized room-temperature reflectance from the (001) face of $(Ph_4P)[Ni(dmit)_2]_3$ and $(Bu_4N)_2[Ni(dmit)_2]_7\cdot 2CH_3CN$ and the (010) face of $(Me_3S)[Ni(dmit)_2]_2$ over the entire spectral range. Data are shown for polarizations parallel and perpendicular to the

TABLE II. Conductivity parameters for $[Ni(dmit)_2]$ salts with closed-shell cations.

Compound	σ_{RT} (Ω^{-1} cm^{-1})	T	E_a (meV)	Ref.
$(Ph_4P)[Ni(dmit)_2]_3$	7	<100 K	10	This work
		>100 K	17	
	10	<125 K	35	9
		>125 K	46	
$(Bu_4N)_2[Ni(dmit)_2]_7\cdot 2CH_3CN$	1		42	This work
	1–10		100–20	10
$(Me_3S)[Ni(dmit)_2]_2$	6.5×10^{-2}		130	This work
$(Ph_4As)[Ni(dmit)_2]_4$	10–15	<160 K	10	24
		>160 K	30	
(tmiz)$[Ni(dmit)_2]$[a]	0.21		110	25
$(Et_4N)[Ni(dmit)_2]$	4×10^{-5}		250	26
$(Et_4N)[Ni(dmit)_2]^2$	4.5×10^{-2}			4
$(Me_4N)[Ni(dmit)_2]$	5×10^{-9}		320	26
$(Pr_4N)[Ni(dmit)_2]$			430	26
$(Bu_4N)[Ni(dmit)_2]$	3×10^{-8}		510	26

[a]tmiz=1,2,3-trimethylimidazolium

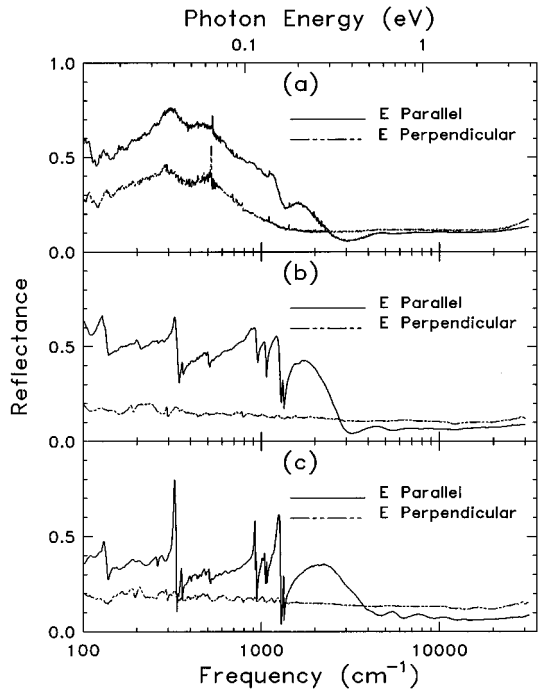

FIG. 5. The polarized reflectance of (a) $(Ph_4P)[Ni(dmit)_2]_3$, (b) $(Bu_4N)_2[Ni(dmit)_2]_7\cdot 2CH_3CN$, and (c) $(Me_3S)[Ni(dmit)_2]_2$ at room temperature for polarization parallel (solid line) and perpendicular (dash-dotted line) to the stacking axis.

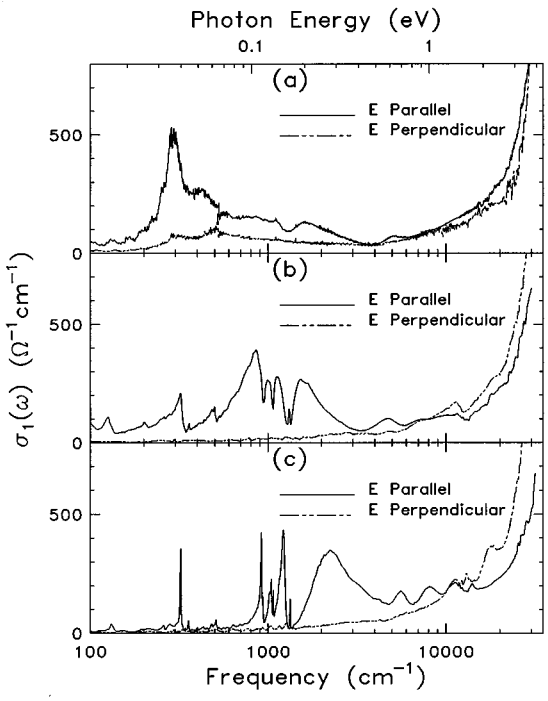

FIG. 6. Frequency-dependent conductivity obtained by Kramers-Kronig analysis of the room-temperature reflectance of (a) $(Ph_4P)[Ni(dmit)_2]_3$, (b) $(Bu_4N)_2[Ni(dmit)_2]_7\cdot 2CH_3CN$, and (c) $(Me_3S)[Ni(dmit)_2]_2$. The conductivity is shown parallel and perpendicular to the stacking axis.

$Ni(dmit)_2$ stacking axis. For the electric field polarized parallel to the stacking direction, a common feature of the three compounds is a value of 40% to 60% in the far to midinfrared with a drop to values of a few percent around 3000 to 4500 cm^{-1}. Superimposed on this reflectance is a series of narrow peaks of varying amplitudes at frequencies typical of molecular vibrations. For higher frequencies, the spectra are almost dispersionless, showing only several weak electronic features. In the case of $(Ph_4P)[Ni(dmit)_2]_3$, such data have been reported over the limited frequency range of 600–25 000 cm^{-1} by Nakamura *et al.*[9] The reflectance values we measured in the region below 1000 cm^{-1} are up to 20% higher than that of Nakamura *et al.*[9] However, the minimum in the reflectance around 3000 cm^{-1} coincides with those previous data.

The reflectance when the polarization is perpendicular to the $Ni(dmit)_2$ stacking axis is also shown in Fig. 5. There is a marked contrast for polarization of the light parallel and perpendicular to the $Ni(dmit)_2$ stacking axis. The reflectivity is low (~15%), flat, and almost featureless for $(Bu_4N)_2[Ni(dmit)_2]_7\cdot 2CH_3CN$ and $(Me_3S)[Ni(dmit)_2]_2$. In contrast, the $(Ph_4P)[Ni(dmit)_2]_3$ perpendicular spectra are similar in shape to that with parallel polarization up to 1000 cm^{-1}, but differs in the deep minimum of the reflectance and in the higher-frequency region.

2. Optical conductivity

The Kramers-Kronig transformation of the stacking-axis reflectance data of Fig. 5 yields the real part of the conductivity $\sigma_1(\omega)$ shown in Fig. 6. The spectra display a broad low-energy band, which contains the largest part of the low-energy oscillator strength and several weak electronic structures at higher frequencies. In all cases they show a conductivity maximum at finite frequency in contrast to the simple Drude behavior of an ordinary metal, which is maximum at $\omega=0$ and then decreases monotonically with increasing frequency. The conductivity maximum shifts to higher frequencies as the dc conductivity decreases. This behavior is in itself suggestive of an optical gap and possibly a transport gap of increasing magnitude. Previous work on $(Ph_4P)[Ni(dmit)_2]_3$ by Nakamura *et al.*[9] found the value of the conductivity at the maximum to be ~140 Ω^{-1} cm^{-1}, about three times smaller than our value of ~520 Ω^{-1} cm^{-1}. This difference is consistent with the fact that the reflectance level we observed in the infrared region is higher than that of Nakamura *et al.*[9]

At low frequency, the spectra exhibit many sharp vibrational features. Several of these modes are A_g vibrations of the $Ni(dmit)_2$ molecule, activated by coupling to the low-energy electronic band.[19] Note that accompanying the shift to higher frequencies of the conductivity maximum, there is an increase of the amplitude of the midinfrared vibrational structures from this electron-molecular-vibration (EMV) coupling. The appearance of these features also changes depending on their frequency location relative to the conductivity maximum. When their frequencies are well below that of the broad maximum they appear as ordinary (Lorentzian) resonances whereas when their frequencies overlap the electronic continuum, they have Fano[29] line shapes: an antiresonance or dip preceded by a peak on the low-frequency side.

Extrapolating the frequency-dependent conductivity to zero frequency, we obtain an estimate of the dc conductivity on the order of $(Me_3S)[Ni(dmit)_2]_2$(<1 Ω^{-1} cm^{-1})<$(Bu_4N)_2[Ni(dmit)_2]_7\cdot 2CH_3CN$(1–5 Ω^{-1} cm^{-1})

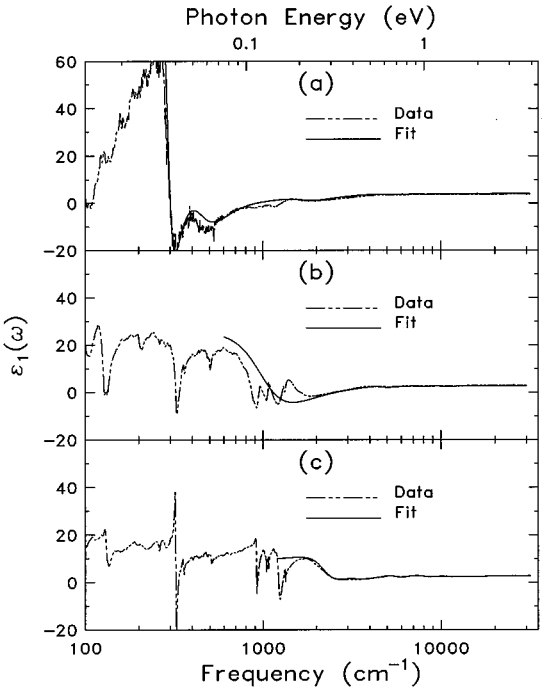

FIG. 7. The real part of the dielectric function (dash-dotted line) obtained by Kramers-Kronig analysis of the room-temperature reflectance of (a) $(Ph_4P)[Ni(dmit)_2]_3$, (b) $(Bu_4N)_2[Ni(dmit)_2]_7\cdot 2CH_3CN$, and (c) $(Me_3S)[Ni(dmit)_2]_2$ along the stacking axis. A Lorentz fit to the reflectance data is shown as the solid lines.

$<(Ph_4P)[Ni(dmit)_2]_3$(5–15 $\Omega^{-1}\,cm^{-1}$) at 300 K. These values are in reasonable agreement with those obtained by four-probe dc measurements (Table II). (We note that the Kramers-Kronig analysis is not too sensitive to conductivities below about 0.1 $\Omega^{-1}\,cm^{-1}$ on account of limits in the accuracy of the reflectance measurements.) An estimate of the semiconducting energy gap is also obtained from the low-energy electronic band shown in Fig. 6. The frequency where the conductivity has risen to half its maximum value yields an estimate of gap values E_g: $(Ph_4P)[Ni(dmit)_2]_3$ ($\sim$270 cm^{-1}=34 meV)$<(Bu_4N)_2[Ni(dmit)_2]_7\cdot 2CH_3CN$ ($\sim$650 cm^{-1}=81 meV)$<(Me_3S)[Ni(dmit)_2]_2$ ($\sim$1750 cm^{-1}=220 meV). These are consistent with transport measurements discussed above which give E_g: $(Ph_4P)[Ni(dmit)_2]_3$ ($\sim$34 meV)$<(Bu_4N)_2[Ni(dmit)_2]_7\cdot 2CH_3CN$($\sim$84 meV) $<(Me_3S)[Ni(dmit)_2]_2$ ($\sim$260 meV).

As expected, the $\sigma_1(\omega)$ for polarization perpendicular to the stacking direction is rather flat. Indeed, the extremely anisotropic behavior in the electronic properties of these $Ni(dmit)_2$ compounds have been observed for many other organic materials as well.[18] Additionally, we note that most of the vibrational lines appear as superimposed bands with no clear evidence for coupling effects. Apart from this, there is little evidence for low-energy electronic absorption perpendicular to the $Ni(dmit)_2$ stacking axis. Only at high frequencies, above 10 000 cm^{-1}, is there electronic absorption.

The real part of the stacking-axis dielectric function, $\epsilon_1(\omega)$, is presented in Fig. 7. A fit of the reflectance data to a Lorentzian model dielectric function is also given. For frequencies near the conductivity maximum, the dielectric function of the three materials displays the usual derivativelike structure. In addition, many of the infrared vibrational excitations result in a negative real dielectric function between the transverse (ω_{TO}) and optical (ω_{LO}) frequency of each mode. The dielectric function of $(Ph_4P)[Ni(dmit)_2]_3$ is negative in the far infrared (characteristic of free carriers), and has a zero crossing around 110 cm^{-1}. The transition across the energy gap is sufficiently strong to give negative values between 300 and 800 cm^{-1}. By extrapolating the low-frequency far-infrared data to zero frequency, we estimate the static dielectric constant for $(Bu_4N)_2[Ni(dmit)_2]_7\cdot 2CH_3CN$ and $(Me_3S)[Ni(dmit)_2]_2$ to be $\epsilon_1(0)\sim 24$ and 8, respectively. We are presently unaware of any microwave measurements of the static dielectric constant in $Ni(dmit)_2$ salts, so comparison with our extrapolated data is not possible.

TABLE III. Parameters of Lorentz fit to the stacking-axis reflectance of $[Ni(dmit)_2]$ salts.

Oscillators	ω_{pj} (cm^{-1})	ω_j (cm^{-1})	γ_j (cm^{-1})
$(Ph_4P)[Ni(dmit)_2]_3$			
1	1380	292	60
2	1765	447	281
3	2517	1000	1356
4	1936	1700	982
5	2100	5000	2000
6	2050	7800	2000
7	2500	11 500	3000
8	1100	15 000	800
$\epsilon_\infty=1.1$			
$(Bu_4N)_2[Ni(dmit)_2]_7\cdot 2CH_3CN$			
1	4900	1050	990
2	2200	4700	1331
3	2286	7300	2023
4	3500	10 000	4500
5	1400	11 700	2000
$\epsilon_\infty=1.19$			
$(Me_3S)[Ni(dmit)_2]_2$			
1	4650	2225	1087
2	2954	3413	1431
3	2900	5560	1355
4	4019	8025	2269
5	5250	11 250	3938
6	1750	14 000	1000
$\epsilon_\infty=1.19$			

3. Dielectric function model

Returning now to the stacking-axis polarization, a quantitative analysis of the reflectance from near-infrared to ultraviolet regions is done by fitting the reflectance [or the complex dielectric function $\epsilon(\omega)=\epsilon_1(\omega)+i\epsilon_2(\omega)$] using a sum of Lorentz oscillators:[23]

$$\epsilon(\omega)=\sum_j \frac{\omega_{pj}^2}{\omega_j^2-\omega^2-i\omega\gamma_j}+\epsilon_\infty, \tag{3}$$

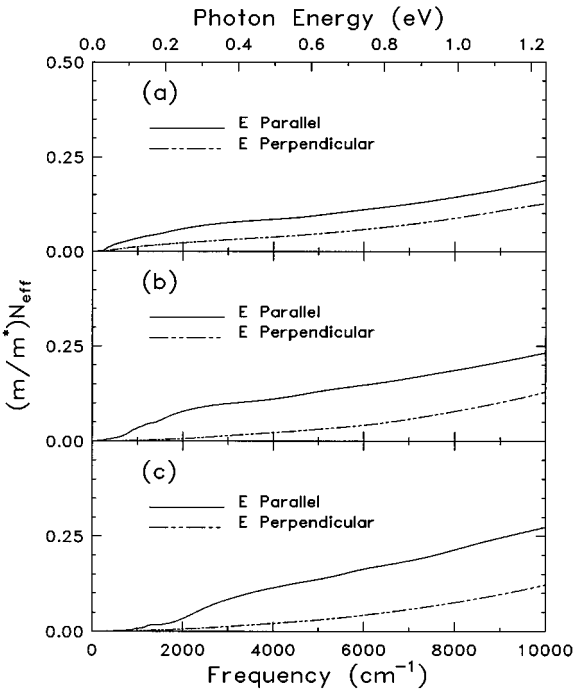

FIG. 8. The sum rule for (a) $(Ph_4P)[Ni(dmit)_2]_3$, (b) $(Bu_4N)_2[Ni(dmit)_2]_7\cdot 2CH_3CN$, and (c) $(Me_3S)[Ni(dmit)_2]_2$ for polarization parallel and perpendicular to the stacking direction.

where ω_{pj}, ω_j, and γ_j are the oscillator strength, center frequency, and scattering rate of the jth transition and ϵ_∞ represents the other higher-frequency contributions to the dielectric function. The parameters obtained for our samples are listed in Table III. The results for the fit are compared to $\epsilon_1(\omega)$ in Fig. 7.

4. Oscillator strength sum rule

Considerable information about the electronic structure of Ni(dmit)$_2$ salts can be extracted from the oscillator strength sum rule.[23] The effective number of electrons participating in optical transitions for energies less than $\hbar\omega$ is given by

$$\left[\frac{m}{m^*}\right]N_{\text{eff}}(\omega)=\frac{m}{32\pi N_c e^2}\int_0^{\omega}\sigma_1(\omega')d\omega', \qquad (4)$$

where m^* is the effective mass of the carriers, m the electronic mass, and N_c the number of Ni(dmit)$_2$ molecules per unit volume. Plots of N_{eff} are shown in Fig. 8.

In the stacking direction, $(m/m^*)N_{\text{eff}}$ at first rises rapidly in the low-frequency region, begins to level off in the near infrared, and then rises again above the onset of the high-frequency electronic bands. From the plateau values of the integrated oscillation strengths in the near infrared, assuming N_{eff} of $(Ph_4P)[Ni(dmit)_2]_3$, $(Bu_4N)_2[Ni(dmit)_2]_7\cdot 2CH_3CN$, and $(Me_3S)[Ni(dmit)_2]_2$ to be 0.33, 0.29, and 0.5, we estimate $m^*=4.17m$, $m^*=2.86m$, and $m^*=4.0m$, respectively. As seen in Fig. 8, below 800 cm^{-1} the stronger oscillator strength of $(Ph_4P)[Ni(dmit)_2]_3$ due to its smaller optical gap is readily evident. In contrast, the enhanced contribution of the midinfrared electronic band is seen in $(Bu_4N)_2[Ni(dmit)_2]_7\cdot 2CH_3CN$. The two curves of $(Ph_4P)[Ni(dmit)_2]_3$ and $(Bu_4N)_2[Ni(dmit)_2]_7\cdot 2CH_3CN$ come together nicely around 20 000 cm^{-1}. In the polarization perpendicular to the stacking axis, $(m/m^*)N_{\text{eff}}$ is small in the infrared but rises rapidly at higher frequencies.

IV. DISCUSSION

A. Electronic features

In principle, the electronic transitions that appear in the $\sigma_1(\omega)$ spectra of these Ni(dmit)$_2$ organic solids will fall into two classes. On the one hand, those at high frequencies generally are the result of localized-excitation bands in the molecule. On the other hand, transitions at lower frequencies that are along the stacking direction will correspond to charge-transfer excitations between the Ni(dmit)$_2$ molecules. The frequencies and oscillator strengths of these charge-transfer bands are clearly related to the electronic structure of the compound, but their interpretation is determined by three types of interactions among the unpaired electrons occupying the highest molecular orbital in the solid. These interactions are the overlap of the electronic wave functions between sites, the Coulomb repulsion of two electrons on the same or adjacent sites, and interactions of the electron with phonons (both lattice vibrations and intramolecular modes of the molecule). Theoretical models for the electronic structure of these materials have emphasized the importance of one or the other of the above interactions, e.g., tight-binding theory,[30] Hubbard model,[31] and Peierls model.[32]

The simple 1:1 ratio of donor-acceptor Ni(dmit)$_2$ salts such as $(Me_4N)[Ni(dmit)_2]$, $(Et_4N)[Ni(dmit)_2]$, $(Pr_4N)[Ni(dmit)_2]$, and $(Bu_4N)[Ni(dmit)_2]$ have one unpaired electron on each Ni(dmit)$_2$ molecule. Because of the large on-site Coulomb repulsion (Hubbard U), these materials display very low dc electrical conductivity at room temperature (Table II). Their electronic structure consists of either completely filled or completely empty bands. Hence, they are often referred to as ''Mott-Hubbard'' insulators. For the complex salts, the most common stoichiometric ratio is 1:2 corresponding to the quarter-filled-band case such as $(Me_3S)[Ni(dmit)_2]_2$, with electrons on average occupying every other site. In this case, it is important to consider an extended Hubbard picture,[31,33–35] which includes hopping from site to site (t), on-site Coulomb repulsion energies (U), nearest-neighbor energy (V_1), and the next-nearest-neighbor energies (V_2). Finally, the behavior of other complex salts, such as $(Ph_4P)[Ni(dmit)_2]_3$ (1:3) or $(Bu_4N)_2[Ni(dmit)_2]_7\cdot 2CH_3CN$ (2:7), is much more complicated than the 1:1 or 1:2 cases.

Let us look first at the simple 1:1 or 1:2 donor-acceptor Ni(dmit)$_2$ salts. An early optical study of $(Bu_4N)[Ni(dmit)_2]$, made by Papavassiliou, Cotsilios, and Jacobsen,[12] shows a low-frequency band at 8850 cm^{-1}. The solution spectra of $[Ni(dmit)_2]^{2-}$ and $[Ni(dmit)_2]^{-}$, reported by Tajima *et al.*,[13] have the lowest intramolecular optical excitation at 8700 cm^{-1}. Due to the symmetry of the molecular orbitals, this transition should be polarized along $[Ni(dmit)_2]$'s molecular long axis. Additional work on the polarized reflectance of OMTSF-$[Ni(dmit)_2]$ (OMTSF: bistetramethylene-TSF) has been reported by Jacobsen *et al.*[16] An interpretation of the spectra is that the charge-transfer excitation is observed at 2600 cm^{-1} and the transitions at 10 000–12 000 cm^{-1}, at 17 000 cm^{-1}, and above may be associated with intramo-

lecular excitons. In contrast, the temperature-dependent polarized reflectance on α-EDT-TTF $[Ni(dmit)_2]$, $(Me_4N)[Ni(dmit)_2]_2$, $(Me_2Et_2N)[Ni(dmit)_2]_2$, and α-$(Et_2Me_2N)[Ni(dmit)_2]_2$, was studied by Tajima *et al.*[14] and Tamura *et al.*[15] In all cases, the measured spectra exhibit a Drude-like shape down to 20 K.

With the above information in mind, let us turn our attention to the frequency-dependent conductivity, $\sigma_1(\omega)$, of the three $Ni(dmit)_2$ compounds shown in Fig. 5 and the fit parameters in Table III. For the typical quarter-filled-band case, such as $(Me_3S)[Ni(dmit)_2]_2$, the midinfrared spectral features in the $Ni(dmit)_2$ stacking direction consist of two strong, broad absorptions. We interpret these bands to be electronic charge transfer between $Ni(dmit)_2$ molecules within the stack. The electronic absorption band at $\sim$2000 cm^{-1} corresponds to the charge transfer: $Ni(dmit)_2^0+Ni(dmit)_2^- \rightarrow Ni(dmit)_2^-+Ni(dmit)_2^0$. The breadth of this band in $(Me_3S)[Ni(dmit)_2]_2$ may result from the overlap of two intratetramer charge-transfer excitations as well as one intertetramer charge-transfer excitation. The energy for this excitation depends on V_1 and hopping integrals, but not on U. The bands at $\sim$5560 and 8000 cm^{-1} are attributed to the charge-transfer process: $Ni(dmit)_2^-+Ni(dmit)_2^- \rightarrow Ni(dmit)_2^0+Ni(dmit)_2^{2-}$. These bands are governed by the Hubbard parameters for on-site (U) and nearest-neighbor (V_1) Coulomb repulsions. Again, the presence of two bands may come from intratetramer and intertetramer charge-transfer excitations.

For the electric field polarized perpendicular to the stacking axis, three absorption bands at $\sim$11 250, 13 000, and 18 000 cm^{-1} are thought to be intramolecular localized excitations or molecular excitons. Note that the energy of the lowest localized excitations is 11 250 cm^{-1} rather than the 8700 cm^{-1} observed in $Ni(dmit)_2$ solution spectra.[13] This blueshift (by $\sim$0.3 eV or 2500 cm^{-1}) is the usual Davydov shift,[36,37] which is expected due to the interaction between the transition dipole moments on adjacent molecules in the dimer. The first two localized excitations are also seen in the parallel polarization on account of the triclinic space group. The fact that in these $Ni(dmit)_2$ salts the molecular plane is not perpendicular to the stacking axis gives rise to a strong coupling and mixing among these intramolecular excitations for two different polarizations.

Despite the significantly different stoichiometric ratios of donor acceptors, the $\sigma_1(\omega)$ spectra of $(Me_3S)[Ni(dmit)_2]_2$, $(Bu_4N)_2[Ni(dmit)_2]_7\cdot 2CH_3CN$, and $(Ph_4P)[Ni(dmit)_2]_3$ are similar in character and typical of semiconducting charge-transfer salts. In the case of $(Bu_4N)_2[Ni(dmit)_2]_7\cdot 2CH_3CN$, the stacking direction has a transition at $\sim$1050 cm^{-1}, attributed as above to charge transfer from a $Ni(dmit)_2$ radical anion to a neutral molecule within a $Ni(dmit)_2$ triad or tetrad. The higher-frequency peaks, at $\sim$4000 and 7300 cm^{-1}, are attributed to charge transfer between two radical $Ni(dmit)_2$ anions. The spectrum perpendicular to the stacking axis shows transitions at $\sim$10 000, 11 400, and 18 700 cm^{-1} which are due to the localized excitation of the isolated $Ni(dmit)_2$ anion. Again, some of these absorption bands are also observed along the stacking axis.

Additionally, in the case of $(Ph_4P)[Ni(dmit)_2]_3$, there are two low-energy electronic excitations (at $\sim$300–450 and 1000–1700 cm^{-1}) for the electric field polarized along the $Ni(dmit)_2$ stacking axis. The structure of this material is unique: two of the three $Ni(dmit)_2$ anions form stacking columns whereas the remaining $Ni(dmit)_2$ anion fills the spaces between the columns. The optical data can be correlated with this structural information. We attribute the 300–450 cm^{-1} peak to charge-transfer excitations within $Ni(dmit)_2$ stacking columns. The higher peak, at $\sim$1000–1700 cm^{-1}, is attributed to a charge transfer to an adjacent neutral molecule. Interestingly, the spectrum perpendicular to the stacking axis displays peaks at similar energies, but has considerably smaller oscillator strength. The bands occurring at $\sim$5000 and 7800 cm^{-1} are attributed to a charge-transfer excitation between $Ni(dmit)_2$ ions. The transitions of an electron excited to a higher orbital or localized excitation are seen to be polarized along both parallel and perpendicular to stacking axis at frequencies of $\sim$11 500 and 15 000 cm^{-1}.

Although these three $Ni(dmit)_2$ compounds have different chemical modifications of the donor cation, an interesting correlation can be made between spectral properties and available structural information. As discussed above, $(Ph_4P)[Ni(dmit)_2]_3$ and $(Bu_4N)_2[Ni(dmit)_2]_7\cdot 2CH_3CN$ have a nearly two-dimensional structure as opposed to the rather quasi-three-dimensional network in $(Me_3S)[Ni(dmit)_2]_2$. The obvious question now is why the increased dimensionality of $(Me_3S)[Ni(dmit)_2]_2$ results in a lower electrical conductivity, a higher activation energy for conduction, and a larger value of optical gap than the other two $Ni(dmit)_2$ salts. In principle, the nature of the donor is primarily responsible for the different manner of stacking in these $Ni(dmit)_2$ materials. It particularly influences the mode of overlap between $Ni(dmit)_2$ molecules. Small cations such as Me_3S^+ promote close-packing arrangements, but also give room for dimerization. Larger ones encourage uniform spacing but also tend to give unusual stoichiometries or packing arrangements. There are always counterexamples; for example, there is a $Ni(dmit)_2$ system with a small cation, $(Me_4N)[Ni(dmit)_2]_2$,[6] that displays metallic electronic properties and becomes superconducting under pressure. In any event, it is clear that the situation is quite complex and that any serious attempt to understand the electronic structure of these $Ni(dmit)_2$ salts needs a careful consideration of the role of both donor and acceptor in the electronic band structure.[38,39]

B. Vibrational features

1. Vibrational mode assignments

We will now turn to a discussion of the vibrational features. In general, the vibrational modes can be divided into two classes. Those involving motion within the $Ni(dmit)_2$ anion itself are classified as intramolecular in nature, whereas the modes involving collective motion of the $Ni(dmit)_2$ anions or the cation stacks are intermolecular or lattice modes. The intramolecular modes occur at high frequencies, and include the totally symmetric phonon modes as well as the infrared allowed modes of B_{1u}, B_{2u}, and B_{3u} symmetry. The intermolecular modes are usually observed at less than 300 cm^{-1}. These modes can be further divided into translational and librational motions. Both types of motion generally occur at low frequencies, some below the frequency range of infrared spectroscopy.

The $Ni(dmit)_2$ molecule possesses a D_{2h} structural symmetry, and has 45 optical modes. These modes may be clas-

TABLE IV. Frequency and assignment of vibrational features in (a) infrared and (b) Raman spectra of $[Ni(dmit)_2]^{n-}$. s: strong; m: medium; sh: shoulder.

$n=2$[a]	$n=2$[b]	$n=1$[a]	$n=0.25$[c]	$n=0$[a]	Assignment
(a) Infrared					
1440 (s)	1430 (s)	1353 (s)	1260	1260 (s)	(C═C)
1065 (s)	1035	1063 (s)	1055	1088 (m)	(C═S)
1034 (s)	1015	1030 (m)		1064 (s)	(C═S)
917 (m)	900 (m)	902 (m)		890 (m)	(C—S)
885 (m)	880 (sh)				(C—S)
472 (m)	455 (m)	498 (m)	495,490	485 (m)	(Ni—S)
311 (m)	310 (m)	317 (s)		328 (m)	(Ni—S)
$n=2$[d]			$n=0.25$[c]		Assignment
(b) Raman					
			2329		
1445			1332		(C═C stretching)
			1075		
1060			1061		
520			494		(ring deformation)
360			364		
320			344		(Ni—S stretching)
			132		

[a]From Ref. 20.
[b]From Ref. 24.
[c]From Ref. 12.
[d]From Ref. 17.

sified into Raman ($8A_g+7B_{1g}+4B_{2g}+2B_{3g}$), silent ($3A_u$), and infrared active ($5B_{1u}+8B_{2u}+8B_{3u}$). The B_{3u} modes are out-of-plane vibrations and are expected to be observed for polarization along the Ni(dmit)$_2$ stacking direction. The B_{1u} and B_{2u} modes are in-plane vibrations and should be seen for polarization in the Ni(dmit)$_2$ molecular plane. Interestingly, the Raman A_g modes are present in the infrared spectrum on account of the strong coupling of these vibrations to the conduction electrons. However, no detailed assignments have yet been made and no one, to our knowledge, has attempted a theoretical normal-mode calculation for the Ni(dmit)$_2$ neutral molecule and Ni(dmit)$_2$ anion. As a basis for discussion, we list in Table IV assignments for the vibrational frequencies in the Ni(dmit)$_2$ system.[12,17,20,24] The assignment of modes in the case of $(Ph_4P)[Ni(dmit)_2]_3$, $(Bu_4N)_2[Ni(dmit)_2]_7\cdot 2CH_3CN$, and $(Me_3S)[Ni(dmit)_2]_2$ is further complicated by the fact that two different Ni(dmit)$_2$ oxidation states contribute to the spectra.

2. Electron-molecular vibration coupling

Figure 9 shows expanded portions of the conductivity spectra in the region where the vibrational features are predominantly found. Table V lists all the features that appear in Fig. 9. As noted in Sec. III B 2 the most important features governing the vibrational spectrum are the location of the main conductivity band (i.e., the existence of an optical gap) and the presence of vibrational structures whose intensities are determined by interactions with the electronic conductivity. In particular, as the principal maximum of the conductivity overlaps with the vibrational frequencies, these EMV effects become increasingly pronounced. In the case of our Ni(dmit)$_2$ compounds, many of these A_g modes are seen as antiresonances whose minima correspond to the vibrational features. Thus, in the presence of the electron-molecular vi-

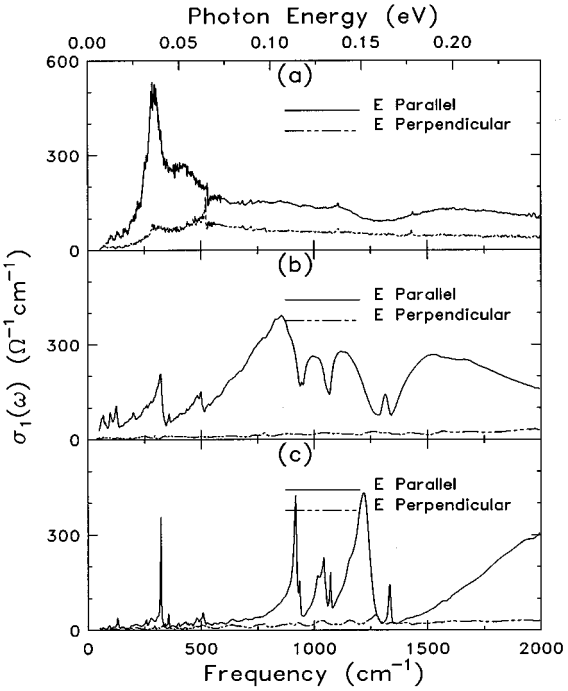

FIG. 9. Expanded portions of the conductivity spectra of (a) $(Ph_4P)[Ni(dmit)_2]_3$, (b) $(Bu_4N)_2[Ni(dmit)_2]_7\cdot 2CH_3CN$, and (c) $(Me_3S)[Ni(dmit)_2]_2$ in the range 0–2000 cm^{-1}.

TABLE V. Observed vibrational frequencies in $[Ni(dmit)_2]$ salts. vs: very strong; s: strong; m: medium; w: weak; vw: very weak; sh: shoulder;*: antiresonance.

Symmetry species	(Ph_4P)			(Bu_4N)			(Me_3S)		
	Freq.	Inten.	Pola.	Freq.	Inten.	Pola.	Freq.	Inten.	Pola.
A_g	1342*	m	$E_\parallel$	1340*,1288*	vs	$E_\parallel$	1333,1207	m,vs	$E_\parallel$
	1063*	w	$E_\parallel$	1069*	vs	$E_\parallel$	1072,1042	m	$E_\parallel$
	941*	vw	$E_\parallel$	953*,939*	s	$E_\parallel$	935,916	m,s	$E_\parallel$
	514*	w	$E_\parallel$	514*	w	$E_\parallel$	508	w	$E_\parallel$
	345*	w	$E_\parallel$	345*	w	$E_\parallel$	356	w	$E_\parallel$
	319*	vw	$E_\parallel$	319*	m	$E_\parallel$	321	s	$E_\parallel$
	139*	w	$E_\parallel$	139*	w	$E_\parallel$	131	w	$E_\parallel$
B_u	1981*	vw	$E_\parallel$	1974*,1974	vw	$E_\parallel,E_\perp$	1960*	vw	$E_\parallel$
	1570*	vw	$E_\parallel$	1572*	vw	$E_\parallel$	1580*	vw	$E_\parallel$
	1431,1425*	vw	$E_\perp,E_\parallel$				1429*	vw	$E_\parallel$
	1107,1097*	vw	$E_\perp,E_\parallel$						
	822*	vw	$E_\parallel$	835*	vw	$E_\parallel$	841	sh	$E_\parallel$
	783	vw	$E_\perp$	783*,781	vw	$E_\parallel,E_\perp$	781	vw	$E_\perp$
	696*,686	vw	$E_\parallel,E_\perp$	696	vw	$E_\parallel$	696	vw	$E_\parallel$
	673*	vw	$E_\parallel$	675*	vw	$E_\parallel$			
	654*	vw	$E_\parallel$	650*	vw	$E_\parallel$	638	vw	$E_\parallel$
	532*,532	vw	$E_\parallel,E_\perp$	538*	vw	$E_\parallel$	528	vw	$E_\parallel$
	497,493*	vw	$E_\perp,E_\parallel$	490*	vw	$E_\parallel$			
	477*,475	vw	$E_\parallel,E_\perp$	479*	vw	$E_\parallel$	480	vw	$E_\parallel$
	440*,439	vw	$E_\parallel,E_\perp$	433*	vw	$E_\parallel$	433	vw	$E_\parallel$
	298*,295	vw	$E_\parallel,E_\perp$	298*,295	vw	$E_\parallel,E_\perp$	294	vw	$E_\perp$
	286,283*	vw	$E_\perp,E_\parallel$	284*	vw	$E_\parallel$	279	vw	$E_\parallel$
				193*, 187	w,vw	$E_\parallel,E_\perp$	192	vw	$E_\parallel$
				109*	m	$E_\parallel$			

bration coupling, the normally infrared-inactive totally symmetric A_g intramolecular vibrational modes become infrared active for electric fields polarized in the direction of the $Ni(dmit)_2$ stacking axis.

The highest-frequency EMV vibrational feature is in the 1300-cm^{-1} range. We have assigned this feature to the C═C stretching A_g mode. It clearly has the effect of producing a broad minimum in $\sigma_1(\omega)$ for $(Ph_4P)[Ni(dmit)_2]_3$ and a deep and strong minimum for $(Bu_4N)_2[Ni(dmit)_2]_7\cdot 2CH_3CN$. For the spectrum of $(Me_3S)[Ni(dmit)_2]_2$ there appears to be a typical Lorentzian-shaped peak. However, the intensity of this peak is far too strong to be an ordinary vibrational peak, and in fact the polarization is also wrong, so we attribute it also to an EMV feature. The line shape is as it is because the main electronic band is at higher frequencies in this compound.

The band near 1070 cm^{-1} is due to EMV coupling of the A_g mode involving C═S stretching. The modes near 940 cm^{-1} are believed to be C—S stretching A_g bands. The remaining features form a group from 100 to 550 cm^{-1}. The bands that are of unambiguous origin are the ring deformation A_g mode near 514 cm^{-1}, the Ni—S stretching A_g mode near 350 and 320 cm^{-1}, and one A_g mode near 139 cm^{-1}.

Apart from the strong features mentioned above, we observe an interesting antiresonance at 514 cm^{-1} for polarization perpendicular to the stacking axis in $(Ph_4P)[Ni(dmit)_2]_3$. We believe that this unusual feature is due to ring deformation of the tetraphenylphosphonium cation. Ordinary infrared-active modes involving C═C at ~1430 cm^{-1} and C═S at ~1100 cm^{-1} are resolved only in $(Ph_4P)[Ni(dmit)_2]_3$. Other infrared-active modes should correspond to Ni—S vibrations near 480 and 330 cm^{-1}. Additional vibrational structures are seen at ~723, 730, and 746 cm^{-1} in $(Ph_4P)[Ni(dmit)_2]_3$ and at ~341 and 400 cm^{-1} in $(Me_3S)[Ni(dmit)_2]_2$ for different polarizations. These features might be due to $Ni(dmit)_2$ modes of other symmetry as well as those of donor cations.

3. Dimer model

We analyze our results for $Ni(dmit)_2$ materials in terms of a model by Rice, Yartsev, and Jacobsen[19] based on isolated dimers. We have fitted this model to the conductivity spectrum of the most insulating of our salts, $(Me_3S)[Ni(dmit)_2]_2$. In this theory, the frequency-dependent conductivity is

$$\sigma(\omega)=-\left(\frac{i\omega e^2a^2N}{4\Omega}\right)\left(\frac{\chi(\omega)}{1-D(\omega)\chi(\omega)/\chi(0)}\right), \qquad (5)$$

where a is the dimer separation, N is the number of dimers per unit cell, and Ω is the volume of the unit cell. The quantity $D(\omega)$ is the phonon propagator

$$D(\omega)=\sum_n \frac{\lambda_n\omega_n^2}{\omega_n^2-\omega^2-i\omega\gamma_n}, \qquad (6)$$

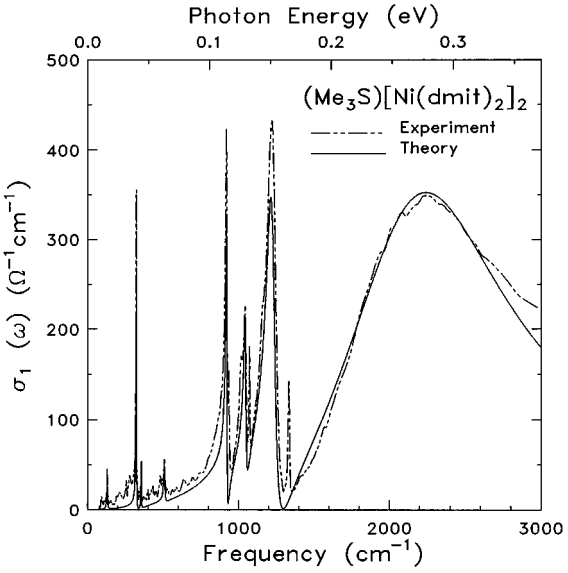

FIG. 10. Isolated dimer fit (solid line) to the frequency-dependent conductivity (dash-dotted line) of $(Me_3S)[Ni(dmit)_2]_2$.

with λ_n the dimensionless electron-phonon coupling constant, ω_n the unperturbed frequency, and γ_n the phonon linewidth for the nth A_g mode. $\chi(\omega)$ is the reduced electronic polarizability,

$$\chi(\omega)=\frac{8t^2/\omega_{ct}}{\omega_{ct}^2-\omega^2-i\omega\gamma_e}, \tag{7}$$

where ω_{ct} is the frequency and γ_e is the linewidth of the electronic charge-transfer excitation. The dimensionless coupling constants are written as

$$\lambda=\chi(0)\,\frac{g_n^2}{\omega_n}=\frac{8t^2g_n^2}{\omega_{ct}^3\omega_n}, \tag{8}$$

where $\chi(0)$ is the zero-frequency limit of Eq. (7). It is the g_n that are the fundamental microscopic electron-molecular-vibration coupling constants.

A fit of this model to the $(Me_3S)[Ni(dmit)_2]_2$ data is shown in Fig. 10. The structural parameters used in the calculation were the separation between the $Ni(dmit)_2$ molecules $a=3.49$ Å and the unit-cell volume $\Omega=1585$ Å^3. The fitted parameters for the charge-transfer band are a transfer integral of $t=1200$ cm^{-1}, a charge-transfer energy of $\omega_{ct}=2180$ cm^{-1}, and an electronic bandwidth of $\gamma_e=1400$ cm^{-1}. The experimental values for the unperturbed phonon frequencies ω_n, EMV coupling constants g_n, and dimensionless electron-phonon coupling constants λ_n are listed in Table VI.

Although the result looks fairly reasonable, it seems that more than one charge-transfer band should be taken into account above 2500 cm^{-1} (see Lorentz fit in Table III). This suggests that $(Me_3S)[Ni(dmit)_2]_2$ should not be considered as an isolated dimer in a $4k_f$ configuration with one electron on two sites. Instead, the interdimer interactions are strong and the $Ni(dmit)_2$ stack is composed of relatively isolated tetramers. The model of electron-molecular vibrational coupling extended by Yartsev[40] to describe isolated tetramers might provide a better agreement with our experimental spectrum.

TABLE VI. Electron-molecular-vibration coupling parameters for $(Me_3S)[Ni(dmit)_2]_2$.

	ω_n[a] (cm^{-1})	g_n (cm^{-1})	λ_n
	1296	330	0.093
	1053	100	0.011
	930	110	0.014
	512	70	0.011
	359	85	0.022
	335	130	0.056
	137	90	0.066
Total			0.274

[a]Obtained from plot of Re[$1/\sigma(\omega)$].

V. SUMMARY

In summary, we have made extensive measurements of the optical and transport properties of $(Ph_4P)[Ni(dmit)_2]_3$, $(Bu_4N)_2[Ni(dmit)_2]_7\cdot 2CH_3CN$, and $(Me_3S)[Ni(dmit)_2]_2$ compounds. The optical properties are dominated by vibrational features at low frequencies and by electronic excitations at higher frequencies. The observed vibrational features include ordinary intramolecular modes and seven ''anomalous'' infrared-active vibrational modes. The latter absorption results from the interaction of these vibrations with the unpaired electron on the $Ni(dmit)_2$ anion. A series of electronic excitations are observed for the electric field polarized along the $Ni(dmit)_2$ stacks. The low-lying peaks are attributed to a charge transfer from one $Ni(dmit)_2$ anion to an adjacent neutral molecule, whereas the excitations higher in frequency are attributed to a charge transfer between two $Ni(dmit)_2$ anions.

We have examined the vibrational modes in these three materials. From analysis of the A_g modes, values for the electron-phonon coupling constants in $(Me_3S)[Ni(dmit)_2]_2$ were obtained. We have also attempted to clarify some of the confusion that exists in the literature by systematically assigning vibrational modes of $Ni(dmit)_2$ molecules in the optical spectra.

Noted added in proof. During publication of this work, we learned via personal communication that the same crystal structure for $(Me_3S)[Ni(dmit)_2]_2$ has been reported by Faulmann *et al.*[41]

ACKNOWLEDGMENTS

We thank J. M. Musfeldt for stimulating discussions. This work was supported by National Science Foundation, Grant No. DMR-9403894, and the Air Force Office of Scientific Research, Grants No. F49620-92-J-0509 and No. F49620-93-I-0322.

[1] J. Ferraris, D. O. Cowan, V. J. Walatka, and J. H. Perlstein, J. Am. Chem. Soc. **95**, 948 (1973).
[2] K. Bechgaard, K. Carueiro, F. B. Rasmussen, G. Rindorf, C. S. Jacobsen, H. J. Pedersen, and J. C. Scott, J. Am. Chem. Soc. **103**, 2440 (1981); K. Bechgaard, C. S. Jacobsen, K. Mortensen, H. J. Pedersen, and N. Thorup, Solid State Commun. **33**, 1119 (1980).
[3] R. P. Shibaeva, V. F. Kaminskii, and E. B. Yagubskii, Mol. Cryst. Liq. Cryst. **119**, 361 (1985); H. Kobayashi, R. Kato, A. Kobayashi, Y. Nishio, K. Kajita, and W. Sasaki, Chem. Lett. **1986**, 789; **1986**, 833; **1986**, 957.
[4] P. Cassoux, L. Valade, H. Kobayashi, A. Kobayashi, R. A. Clark, and A. E. Underhill, Coord. Chem. Rev. **110**, 115 (1991).
[5] L. Brossard, M. Ribault, L. Valade, and P. Cassoux, Physica B **143**, 378 (1986).
[6] K. Kajita, Y. Nishio, S. Moriyama, R. Kato, H. Kobayashi, W. Sasaki, A. Kobayashi, H. Kim, and Y. Sasaki, Solid State Commun. **65**, 361 (1988).
[7] H. Tajima, M. Inokuchi, A. Kobayashi, T. Ohta, R. Kato, H. Kobayashi, and H. Kuroda, Chem. Lett. **1993**, 1235.
[8] A. E. Pullen, J. Piotraschke, K. A. Abboud, J. R. Reynolds, H. L. Liu, and D. B. Tanner, Polym. Mater. Sci. Eng. Symp. Proc. **72**, 321 (1995).
[9] T. Nakamura, A. E. Underhill, T. Coomber, R. H. Friend, H. Tajima, A. Kobayashi, and H. Kobayashi, Inorg. Chem. **34**, 870 (1995); T. Nakamura, A. E. Underhill, T. Coomber, R. H. Friend, H. Tajima, A. Kobayashi, and H. Kobayashi, Synth. Met. **70**, 1061 (1995).
[10] L. Valade, J.-P. Legros, M. Bousseau, P. Cassoux, M. Garbauskas, and L. V. Interrante, J. Chem. Soc. Dalton Trans. **1985**, 783.
[11] R. Kato, H. Kobayashi, H. Kim, A. Kobayashi, Y. Sasaki, T. Mori, and H. Inokuchi, Synth. Met. **27**, B359 (1988).
[12] G. C. Papavassiliou, A. M. Cotsilios, and C. S. Jacobsen, J. Mol. Struct. **15**, 41 (1984).
[13] H. Tajima, T. Naito, M. Tamura, A. Kobayashi, H. Kuroda, R. Kato, H. Kobayashi, R. A. Clark, and A. E. Underhill, Solid State Commun. **79**, 337 (1991).
[14] H. Tajima, M. Tamura, T. Naito, A. Kobayashi, R. Kato, H. Kobayashi, R. A. Clark, and A. E. Underhill, Mol. Cryst. Liq. Cryst. **181**, 233 (1990).
[15] M. Tamura, R. Masuda, T. Naito, H. Tajima, H. Kuroda, A. Kobayashi, K. Yakushi, R. Kato, H. Kobayashi, M. Tokumoto, N. Kinoshita, and H. Anzai, Synth. Met. **41**, 2499 (1991).
[16] C. S. Jacobsen, V. M. Yartsev, D. B. Tanner, and K. Bechgaard, Synth. Met. **55**, 1925 (1993).
[17] W. J. Barreto, M. C. C. Ribeiro, and P. S. Santos, J. Mol. Struct. **269**, 75 (1992).
[18] D. B. Tanner, in *Extended Linear Chain Compounds*, edited by J. S. Miller (Plenum, New York, 1982), Vol. 2, Chap. 5.
[19] M. J. Rice, V. M. Yartsev, and C. S. Jacobsen, Phys. Rev. B **21**, 3437 (1980).
[20] G. Steimecke, H. J. Sieler, R. Kirmse, and E. Hoyer, Phosphorus and Sulfur **7**, 49 (1979).
[21] Robertson Microlit Lab, Inc., Madison, NJ.
[22] G. M. Sheldrick, SHELXTL plus; Nicolet XRD Corporation, Madison, Wisconsin (1990).
[23] F. Wooten, in *Optical Properties of Solids* (Academic, New York, 1972).
[24] L. Valade, J.-P. Legros, and P. Cassoux, Mol. Cryst. Liq. Cryst. **140**, 335 (1986).
[25] D. Reefman, J. P. Cornelissen, J. G. Haasnoot, R. A. G. de Graafi, and J. Reedijk, Inorg. Chem. **29**, 3933 (1990).
[26] G. J. Kramer, J. C. Jol, H. B. Brom, L. R. Groeneve, and J. Reedijk, J. Phys. C **21**, 4591 (1988).
[27] A. J. Epstein, E. M. Conwell, D. J. Sandman, and J. S. Miller, Solid State Commun. **23**, 355 (1977).
[28] A. J. Epstein, E. M. Conwell, D. J. Sandman, and J. S. Miller, Solid State Commun. **24**, 627 (1977).
[29] U. Fano, Phys. Rev. **124**, 1866 (1961).
[30] J. M. Ziman, in *Principles of the Theory of Solids*, 2nd ed. (Cambridge University Press, Cambridge, England, 1972).
[31] J. Hubbard, Phys. Rev. B **17**, 494 (1978).
[32] R. E. Peierls, in *Quantum Theory of Solids* (Oxford University Press, London, England, 1955), p. 108.
[33] S. Mazumdar and Z. G. Soos, Phys. Rev. B **23**, 2810 (1981).
[34] S. Mazumdar and A. N. Bloch, Phys. Rev. Lett. **50**, 207 (1983).
[35] J. E. Hirsch and D. J. Scalapino, Phys. Rev. Lett. **50**, 1168 (1983).
[36] A. S. Davydov, in *Theory of Molecular Excitons* (Plenum, New York, 1971).
[37] D. P. Craig and S. H. Walmsley, in *Excitons in Molecular Crystals* (Benjamin, New York, 1971).
[38] A. Kobayashi, H. Kim, Y. Sasaki, R. Kato, and H. Kobayashi, Solid State Commun. **62**, 57 (1987).
[39] E. Canadell, S. Ravy, J. P. Pouget, and L. Brossard, Solid State Commun. **75**, 633 (1990).
[40] V. M. Yartsev, Phys. Status Solidi B **126**, 501 (1984); **49**, 157 (1988).
[41] C. Faulmann, A. Errami, B. Donnadieu, J.-P. Legros, I. Malfant, P. Cassoux, M.-C. Rovira, and E. Canadell (unpublished)